Investigation of temperature coefficients of PV modules through field measured data

Basant Raj Paudyal [*], Anne Gerd Imenes

University of Agder, Faculty of Engineering and Science, Grimstad, Norway

ARTICLE INFO

ABSTRACT

Varying broadband irradiance and temperature are generally known as the major factors influencing the performance of PV modules, but studies have also shown the substantial impact of spectral variations. In this work, a simple and efficient method to calculate the temperature coefficient using long term data is demonstrated. Temperature coefficients of PV modules are estimated from long term performance data following IEC 60891 standard with additional spectral correction, and are compared against the datasheet values. Significant improvement of correlation coefficient from -0.89 to -0.97 is observed during the regression for maximum power temperature coefficient of two poly-crystalline modules, after spectral correction by spectral factor (SF). Also, the standard deviation of yearly estimated values of these coefficients reduced from 5–7 % to 1–2 %. In another setup involving spectral measurements and various PV technologies, the annual mean of 1.62 eV for average photon energy in 350–1700 nm range, suggests a general blue shift of the spectrum. Higher averages than reference values of useful fraction (UF) for c-Si, CIGS and HIT technologies also validate the blue shift of spectrum. Results show SF produces maximum power temperature coefficients closer to the datasheet values compared to UF, suggesting better applicability of SF as an index for spectral correction. The coefficient values were found closer to STC values and the results from Mann and Kendall test, employed to detect any underlying monotonic trend in the development of temperature coefficients over eight years, showed no increasing or decreasing trend and hence no degradation of temperature coefficients for the long-term exposed PV modules.

1. Introduction

The global photovoltaic (PV) community uses Standard Test Conditions (STC) to rate the electrical parameters of PV modules. The STC power rating of PV modules makes it easier to perform a direct comparison of different PV modules installed in a particular location, or intercomparisons between different locations. The performance of PV modules is dependent on ambient conditions, with major impacts caused by irradiance and temperature (Ziane et al., 2021). While the PV power output increases with increasing irradiance for all technologies, it decreases with the increase in module temperature for most technologies. Apart from these two major factors, mounting geometry, spectral and angle of incidence effects are also known to play part in performance variations (Tayyib et al., 2014; Dubey et al., 2015; Sharma et al., 2017; Goossens et al., 2018; Simioni and Schaeffer, 2019). These effects are carefully considered while rating the modules in controlled indoor conditions, so these parameters need to be monitored in outdoor conditions as well to quantify the impacts on module performance. Thus,

the module current–voltage (I- V) characteristics taken in the field, need to be corrected closer to STC (same conditions as when PV modules are rated), for the accurate outdoor performance analysis of PV modules.

The performance of installed PV modules carries a warranty and needs to be assessed while in service, which necessitates the measurement of performance data in the field. Since it is not possible to maintain the temperature at the STC value (25°C) during measurements in the field, it is necessary to correct the measured I-V data to STC by using temperature coefficients. A detailed mathematical explanation of temperature coefficients of various electrical parameters is provided in (Berthod et al., 2016; Mitterhofer et al., 2019).

1.1. PV module temperature coefficients

In the ideal case, the energy conversion efficiency of PV devices is limited by fundamental loss mechanisms (Henry, 1980). These range from thermalisation loss (due to inefficient utilization of high energy photons), transmission loss (due to non-absorption of photons below the bandgap), emission loss (originating from the radiative emissions of the

Nomenclature

AM	Air Mass
APE	Average Photon Energy
CIGS	Copper indium gallium selenide
CdTe	Cadmium telluride
DNI	Direct normal irradiance
FF	Fill factor
GHI	Global horizontal irradiance
GW	Giga Watt
HIT	Heterojunction with intrinsic thin layer
$I-V$	Current–Voltage
IEC	International Electrotechnical Commission
I_{MP}	Current at maximum power
I_{SC}	Short circuit current
MK	Mann and Kendall
MPP	Maximum power point
POA	Plane of Array
PR	Performance Ratio
PV	Photovoltaics
P_{MAX}	Maximum Power
SF	Spectral Factor
SR	Spectral Response
STC	Standard Test Conditions
UF	Useful Fraction
UV	Ultra violet
V_{MP}	Voltage at maximum power
V_{OC}	Open circuit voltage
$a-Si$	Amorphous silicon
$c-Si$	Crystalline silicon
A	Effective area of PV device
$E(\lambda)$	Solar irradiance at specific wavelength λ
$E_{REF}(\lambda)$	Spectral irradiance of standard AM1.5G spectrum
E_{g0}	Energy bandgap at absolute zero temperature
E_g	Energy bandgap
G	Solar irradiance
G_{STC}	Solar irradiance at STC conditions
$I_{SC,ideal}$	Ideal short circuit current
I_{ph}	Photo-generated current
N_s	No. of cells in the module
P	Computed probability value
R^2	Coefficient of determination
R_{sh}	Shunt resistance
R_s	Series resistance
S	MK Statistic
SR_{REF}	Spectral response of the reference device
T	Temperature
T_c	Cell temperature
UF_{REF}	Reference UF value for a given PV material under AM1.5G Spectrum
Z	MK Statistic
c	Speed of light in vacuum
f_c	Collection fraction
h	Planck's constant
k	Boltzmann's constant
m	Diode ideality factor
q	Elementary charge
Φ	Significance level
α	Temperature coefficient of I_{SC}
β	Temperature coefficient of V_{OC}
δ	Magnitude of the trend in MK test
γ	Temperature coefficient of P_{MAX}
κ	Temperature coefficient of FF
λ	Wavelength
μ	Mean
ϕ	Photon flux
σ	Standard deviation

device), angular mismatch loss (due to the mismatch in absorption and emission of light), and Carnot losses (arising from the conversion of thermal energy in radiation to the electrical energy in a PV device). The theoretical efficiency limits of single junction devices were first calculated by Shockley and Queisser using the detailed balance principle (Shockley and Queisser, 1961), thus the name Shockley-Queisser limit. In real devices also radiative recombination, optical loss, and parasitic resistance losses are present.

The above-mentioned losses are discussed in detail in (Dupré et al., 2015; Mitterhofer et al., 2019). The negative impacts caused by increasing temperature on these loss mechanisms has been understood for PV devices (Green, 1982). The dependence on the temperature is represented by the temperature coefficients, which are approximately linear for the electrical parameters of the PV cell (Dubey et al., 2015; Dupré et al., 2015; Duck et al., 2018). For this reason, linear regression can be used to experimentally determine the temperature coefficients of the PV parameters (Riesen et al., 2016). Usually the temperature coefficients of PV modules are provided by the manufacturers in the datasheet. These values are measured under controlled indoor conditions, defined by the international standard IEC 60891 (IEC, 2009). However, the temperature coefficients provided by the manufacturer are not always accurate as deviations are reported in literature (Allet et al., 2011; Figgis and Abdallah, 2019). PV modules are deployed outdoors, which exposes them to various factors causing material and performance degradation. The outdoor degradation mechanisms are well documented but the underlying causes of these degradation modes are yet to be completely understood (Kontges et al., 2014). Also, the impact of various degradation modes on temperature coefficients and the

degradation of the coefficients themselves after years of operation are not properly investigated or understood (Mitterhofer et al., 2019). It is speculated that the PV module temperature coefficients also tend to degrade over the exposure time (Dubey et al., 2015), but not enough evidence is yet available.

1.1.1. Temperature coefficient of short circuit current

The short circuit current of PV devices, I_{SC}, tends to increase with increasing temperature. This is due to the energy bandgap of such devices being reduced at higher temperatures, with a corresponding rise of the band-to-band absorption coefficient across the spectrum (Green, 2003). Hence, the temperature coefficient of short circuit current, α, is dependent on the energy bandgap E_g and the incident spectrum (Dupré et al., 2015) as defined by Eq. (1).

$$\alpha = \frac{1}{I_{SC}} \frac{dI_{SC}}{dT} = \frac{1}{I_{SC,ideal}} \frac{dI_{SC,ideal}}{dE_g} \frac{dE_g}{dT} + \frac{1}{f_c} \frac{df_c}{dT} \quad (1)$$

where $I_{SC,ideal}$ is the ideal short circuit current, T is the temperature, and f_c is the collection fraction. The ideal short circuit current is calculated from the product of the elementary charge q and the integral photon flux density of the incident spectrum limited by the energy band gap at cell temperature T_c. The collection fraction refers to how much of the ideal current is collected by the PV cell and depends on reflection, transmission, and parasitic absorption of the cell (Dupré et al., 2015).

The determination of α from an indoor setup presents a challenge, as solar simulators often do not provide the exact similar spectrum as the reference AM1.5G spectrum. The IEC standard for solar simulators states

that the standard deviation of spectral variation must be within 25 % at all wavelength intervals from 400 nm to 1100 nm (IEC, 2020). This introduces significant uncertainty in the temperature coefficient determination from indoor laboratory tests, which is the reason for the variation found in α values (Landis, 1994). A similar issue arises in an outdoor test facility if spectral irradiance is not carefully monitored with a calibrated broadband spectrometer. Due to the varying incident spectrum, it is difficult to accurately calculate α when plotting large outdoor datasets of I_{SC} versus temperature, as large scatter is observed around the trend-line.

1.1.2. Temperature coefficient of open circuit voltage

The open circuit voltage of a PV device, V_{OC}, represents a condition where the total rate of photogeneration and the rate of recombination are equal such that there is no current flow in the circuit (Dupré et al., 2015). While the photogeneration rate depends on the incident spectrum and absorption of the photons, the recombination rate is closely related to the temperature. The temperature coefficient of open circuit voltage, β, accounts for 80–90 % of the total temperature coefficient for maximum power in PV devices not affected by parasitic resistances and fill factor losses (Green, 2003). Referring to Eq. (2), the temperature coefficient of V_{OC} can be calculated assuming a linear variation of E_g on the temperature range of interest (Dupré et al., 2015).

$$\beta = \frac{1}{V_{OC}} \frac{dV_{OC}}{dT} = \frac{1}{V_{OC}} \frac{1}{T_c} \left(V_{OC} - \frac{E_{g0}}{q} - \gamma_r \frac{kT_c}{q} \right) \tag{2}$$

where E_{g0} refers to the band gap linearly interpolated to absolute zero temperature, k is the Boltzmann constant, and the coefficient γ_r relates to the dominant recombination processes in the cell (Dupré et al., 2015; Senturk, 2020). The γ_r-term is the least important of the three terms in Eq. (2), accounting for only 0–10 % of β in example calculations based on experimental values of c-Si cells presented by Dupré et al. (2015).

1.1.3. Temperature coefficient of maximum power

The most widely used temperature coefficient in performance studies of PV modules is the maximum power (P_{MAX}) temperature coefficient, γ. This value is used to correct module power to the STC level and calculate the temperature corrected performance ratio. The general equation for the temperature coefficient of P_{MAX} is given as (Dupré et al., 2015)

$$\gamma = \alpha + \beta + \kappa \tag{3}$$

where α, β and κ are the temperature coefficients for the short circuit current, open circuit voltage and fill factor respectively. Fill factor (FF) is given as the ratio of maximum power to the product of I_{SC} and V_{OC}. Fill factor is mostly affected by the parasitic resistances in the solar cell. Higher value of FF, achieved through high values of shunt resistance (R_{sh}) and minimal series resistance (R_s), denotes a higher efficiency of the cell.

1.2. Temperature coefficient measurements: IEC 60891 standard

Temperature coefficient measurements can be performed indoors using a solar simulator or outdoors using natural sunlight, closely following the recommendations from the IEC 60891 standard (IEC, 2009). If a solar simulator is used, it should comply with class BBB (spatial non-uniformity of irradiance up to 5 %, short term and long instability of irradiance at 2 % and 5 % respectively) or better in accordance with IEC 60904–9. During the indoor measurement of temperature coefficients, the PV cells are usually placed on a temperature-controlled setup. The cells are illuminated with the solar simulator, and subsequent current–voltage (I-V) curves are measured over a range of cell temperatures (King et al., 1997; Tayyib et al., 2014; Dubey et al., 2015). The module temperature should be stable within $\pm$ 2 °C before the measurement routine, and the range of temperatures should span at least 30 °C.

For outdoor measurements, the irradiance should ideally be stable with short-term oscillations caused by clouds, smoke or haze being less than $\pm$ 2 % of the total irradiance as measured by the reference device. Wind-speed should be less than 2 ms^{-1}. Spectral variations should be accounted for either by performing the experiment within a short period or time, or by applying spectral corrections for longer periods of measurements. The PV module under test should initially be shielded from sun and wind such that the temperature is within $\pm$ 2 °C of the ambient air temperature. When the module is uncovered, it starts heating up and the I-V characteristics and module temperature should be recorded in parallel. Also, the module can be cooled down to a required temperature and allowed to warm up naturally. The irradiance as measured by the reference device should remain constant within $\pm$ 1 % during the recording period for each I-V curve data set. It is required that the temperature range is at least 30 °C, spanned across at least four approximately equal increments.

The measured values of I_{SC}, V_{OC} and P_{MAX} are plotted as functions of the module temperature. A least-squares-fit curve is fitted through each data set, and the slopes for current, voltage and power give the values for α, β and γ for the module. It should be noted that the temperature coefficients are valid at the irradiance level and spectrum at which they were measured, but data can be translated to other irradiance levels within the range where the module is linear (IEC, 2009).

1.3. PV performance evaluation

Performance ratio (PR) is an indicator prescribed in IEC 61724–1 (IEC, 2017; Malvoni et al., 2020) for the analysis of energy delivered by PV modules. For market dominant crystalline silicon modules, the impact of temperature variation is found to be significant, as a clear drop in PR values is recorded in warmer temperature conditions (Silverman et al., 2014). This is an opposite trend to the array yield, which increases due to improved irradiance conditions during the warmer summer periods in most regions across the globe.

The calculation of the PV performance indicator PR involves a comparison with the reference yield, which is calculated from the measured in-plane irradiation relative to the STC irradiance. Temperature is found to be the leading effect for variations in performance ratio, as it is found to account for around 85 % of the observed effect on global average of PR for crystalline silicon modules (Peters and Buonassisi, 2021). Thus, it is common to also calculate the temperature-corrected PR value, referring to the STC conditions (Dierauf et al., 2013; Herteleer et al., 2017), and in some cases spectral corrections are also included (Ishii et al., 2011; Paudyal and Imenes, 2019).

PV modules are known to suffer from various degradation modes, caused by physical and chemical processes during their lifetime. Different stages of degradation appear during the early, middle and end-of-life stages of the PV modules (Kontges et al., 2014). Investigation of degradation of temperature coefficients is necessary as these coefficients are the basis of temperature correction of module parameters to STC conditions. Any deviation from the actual temperature coefficient values would then translate to errors in PR calculations and finally into mismatch between modeled and measured performance statistics. This mismatch, when translated to the multi-GW scale PV power plants, would incur a large amount of financial loss.

Spectral effects are usually quantified using spectral irradiance readings integrated over a certain wavelength range. Due to costly and complex instrumentation, these readings are not easily available. Authors in (Ishii et al., 2011; Alonso-Abella et al., 2014) propose the use of short circuit measurements to deduce the spectral factor values similar to the relation defined in the IEC60904-7 standard in absence of spectral irradiance measurements. Among the indices that are used to quantify the spectral impact, average photon energy is identified to better indicate spectral shift of the incident irradiation to blue or red rich wavelength region compared to other available spectral indices. Meanwhile, among the PV device dependent spectral indices, useful fraction is found

to perform better than other spectral indicators (Louwen et al., 2016). These indices are defined in Section 2.1 below.

As there is limited literature available on the development of temperature coefficients over the lifetime of PV modules, this article attempts to contribute to the existing knowledge in this area. A general method is proposed that is applicable for systems with long term performance monitoring facilities, to enable the analysis of the degradation of temperature coefficients of the module I-V curve characteristics over a timescale of years.

2. Method of analysis

2.1. Spectral impact quantification

The spectral impact on PV devices can be quantified using different indices according to the availability of spectroradiometer data (Rodrigo et al., 2017). Average photon energy (APE) is an index that is dependent on the chosen reference wavelength range of the measured spectrum, and is independent of the PV device spectral response range. APE quantifies whether the solar spectrum is "blue-rich" or "red-rich" compared to a reference spectrum. APE expressed in electron volts (eV) is calculated as (Minemoto et al., 2007):

$$APE = \frac{\int_{\lambda_1}^{\lambda_2} E(\lambda)d\lambda}{q \int_{\lambda_1}^{\lambda_2} \phi(\lambda)d\lambda} \tag{4}$$

where $E(\lambda)$ is the solar irradiance at a specific wavelength λ, $\phi(\lambda)$ is the spectral photon flux density, and λ_1 and λ_2 are the lower and upper limits of the wavelength range in consideration. For the two different wavelength ranges 350–1050 nm and 350–1700 nm, the corresponding APE values for the AM1.5G reference spectrum are 1.88 eV and 1.59 eV, respectively. The photon flux density is given as:

$$\phi(\lambda) = \frac{E(\lambda)}{hc/\lambda} \tag{5}$$

where h is the Planck's constant, and c is the speed of light in vacuum.

Useful fraction (UF) is an index that is dependent on the wavelength range of the measured spectrum and the PV device spectral response range. The UF is a PV device dependent parameter and has a specific reference value for the individual PV device. It is expressed as (Betts et al., 2004):

$$UF = \frac{\int_{\lambda_0}^{\lambda_g} E(\lambda)d\lambda}{\int_{\lambda_1}^{\lambda_2} E(\lambda)d\lambda} \tag{6}$$

where λ_1 and λ_2 are, as before, the wavelength range limits of irradiance under consideration, whereas λ_0 and λ_g are the lower and upper (bandgap) absorption wavelength limits of the PV device spectral response.

The short circuit current of a PV device under illumination is quantified as in (Luque and Hegedus, 2011):

$$I_{SC} = A \int_{\lambda_0}^{\lambda_g} E(\lambda)SR(\lambda)d\lambda \tag{7}$$

where A is the effective area of the PV device, and $SR(\lambda)$ is the spectral response of the same PV device. The spectral response (SR) is determined by the band gap, cell thickness and transport in the material (Eke et al., 2017), and is defined as the ratio of wavelength dependent photo-generated current $(I_{ph}(\lambda))$ to the incident spectral irradiance on the device area:

$$SR = \frac{I_{ph}(\lambda)}{AE(\lambda)} \tag{8}$$

Spectral factor (SF) is another index that is used to quantify the spectral

impact on PV devices. In this case, the spectral variation is quantified with respect to a reference device of known spectral response. If both spectral irradiance and spectral response of the given PV device is available, the SF can be calculated as (IEC, 2019):

$$SF = \frac{\int E_{REF}(\lambda)SR(\lambda)d\lambda / \int E(\lambda)SR(\lambda)d\lambda}{\int E_{REF}(\lambda)SR_{REF}(\lambda)d\lambda / \int E(\lambda)SR_{REF}(\lambda)d\lambda} \tag{9}$$

where $E_{REF}(\lambda)$ is the spectral irradiance of the standard AM1.5G reference spectrum, and SR_{REF} is the spectral response of the reference device. The reference device and the PV device under consideration can have different ranges of spectral absorption limits. If spectral irradiance measurements are unavailable but irradiance data can be obtained from a pyranometer, the SF can be computed assuming the pyranometer as a reference device. A broadband pyranometer with spectral range up to 2800 nm or above (class A pyranometer according to the IEC 61724–1 standard) is sensitive to more than 99 % of the total integrated AM1.5G spectrum (G_{STC}), much above the active region of commercially available PV materials. The ISO 9060:1990 standard requires the pyranometers to respond evenly within the 300–2800 nm range, thus the pyranometers can be considered as spectrally flat. In Eq. 9, the total integrated energy content of the reference device therefore becomes the broadband irradiance measured by the pyranometer (G) and the spectral response becomes unity. The expression of SF can then be rewritten as:

$$SF = \frac{I_{SC}}{I_{SC(STC)}} \left(\frac{G_{STC}}{G}\right) \tag{10}$$

2.2. STC corrections

The corrections to STC irradiance conditions are performed using the following equations (Mitterhofer et al., 2019; Siddique et al., 2013), where N_S is the number of cells in the module and m is the diode ideality factor, which is here considered as 1 for simplicity:

$$I_{SC(CORR)} = \left(\frac{G_{STC}}{G}\right) I_{SC} \tag{11}$$

$$V_{OC(CORR)} = V_{OC} - N_s \frac{mkT}{q} \ ln\left(\frac{G}{G_{STC}}\right) \tag{12}$$

$$P_{MAX(CORR)} = \left(\frac{G_{STC}}{G}\right) P_{MAX} \left(\frac{1}{SF}\right) \tag{13}$$

For data collected in setup 1 (see Section 3.1), Eq. 13 includes the SF term for spectral correction. For data collected in setup 2, the spectral corrections are instead performed using UF as given by the following equations for short circuit current and maximum power (where open circuit voltage is still given by Eq. 12 above):

$$I_{SC(CORR)} = \left(\frac{G_{STC}}{G}\right) I_{SC} \left(\frac{UF_{REF}}{UF}\right) \tag{14}$$

$$P_{MAX(CORR)} = \left(\frac{G_{STC}}{G}\right) P_{MAX} \left(\frac{UF_{REF}}{UF}\right) \tag{15}$$

Here, UF_{REF} signifies the reference useful fraction value for the given PV material under the AM1.5G spectrum. The reference UF value for each material technology evaluated in this paper is presented in Table 1.

For the analysis of outdoor data, the short circuit current, open cir-

Table 1
Reference UF value for various PV devices.

PV material	SR range (nm)	UF_{REF}
c-Si	350–1150 (Magare et al., 2016)	0.85
HIT	350–1200 (Magare et al., 2016)	0.87
CIGS	350–1300 (Müllejans et al., 2004)	0.91

cuit voltage and maximum power of each module are plotted against the module temperature for in-plane irradiance values above 400 Wm^{-2}. The I_{SC}, V_{OC} and P_{MAX} values are corrected for irradiance and also spectral variations wherever possible, by using APE and SF to correct to the STC reference values. Finally, the temperature coefficients are calculated by evaluating the slope of the regression line formed by the scatter plot of electrical parameters and module temperatures.

2.3. Mann and Kendall test

The Mann and Kendall (MK) test is a statistical method for the trend analysis of time series of non-parametric data (Mann, 1945; Kendall, 1975). This is a widely used trend analysis technique in climatology and hydrology. The MK test is performed to assess if there is a monotonic upward or downward trend for a particular variable over the time series. The null hypothesis of this test indicates no trend, while the alternative hypothesis indicates the presence of a trend. The test compares the relative magnitudes of sample data rather than the data values themselves (Gilbert, 1987). It is required that the times series should not contain any kind of serial correlation for performing the MK test. The MK statistic S is estimated as:

$$S = \sum_{k=1}^{n-1} \sum_{j=k+1}^{n} sgn(X_j - X_k) \qquad (16)$$

where X_j and X_k are sequential data values and n is the total number of data points in the data series. The sign function $sgn(X_j - X_k)$ is defined in Eq. (17):

$$sgn(X_j - X_k) = \begin{cases} 1 & \text{if } sgn(X_j - X_k) > 0 \\ 0 & \text{if } sgn(X_j - X_k) = 0 \\ 0 & \text{if } sgn(X_j - X_k) < 0 \end{cases} \qquad (17)$$

Eqs. 16,17 can be used to calculate the MK statistics for cases where the number of observations (n) is less than 8 (Wang et al., 2020; Blain, 2015). If $n \geqslant 8$, the statistic S approximates the normal distribution and provided that the mean of S is zero, the variance of S is calculated as (Gilbert, 1987; Wang et al., 2020):

$$Var(S) = \frac{1}{18}\left[n(n-1)(2n+5) - \sum_{m=1}^{g} t_m(t_m-1)(2t_m+5)\right] \qquad (18)$$

where n is total number of data points, g is the number of tied groups (defined as a data point having more than one occurrence in the time series, which is not the case in this study), and t_m is the number of data points in the mth group. The MK statistic Z is in this case of normal distribution given by,

$$Z = \begin{cases} \dfrac{S-1}{\sqrt{Var(S)}} & \text{if } S > 0 \\ 0 & \text{if } S = 0 \\ \dfrac{S+1}{\sqrt{Var(S)}} & \text{if } S < 0 \end{cases} \qquad (19)$$

For a trend to be said increasing, the Z value is positive and the computed probability (P value) should be greater than the level of significance. Similarly, for the decreasing trend, the Z value is negative and the P value should be greater than the level of significance. Finally, there is no trend when the P value is less than the level of significance. Here, for a confidence interval of 95 % and significance level $\varphi = 5\%$, a positive Z value larger than $Z(1 - \varphi/2) = 1.96$ shows a significant increasing trend, while a negative Z value lower than -1.96 shows a significant decreasing trend. With less confidence it can be concluded that $Z > 0$ indicates an increasing trend and $Z < 0$ indicates a decreasing trend. While the MK test denotes the trend of the data, the magnitude of the trend (δ) can be quantified by using a non-parametric procedure described by (Sen, 1968):

$$\delta = median\left(\frac{X_j - X_k}{t_j - t_k}\right) \qquad (20)$$

where X_j and X_k are the data values at time t_j and t_k respectively.

3. Experimental details

3.1. The outdoor test facility

The PV measurements for this study were performed at the Grimstad campus of University of Agder, Norway as described in (Imenes et al., 2011; Paudyal and Imenes, 2019). This study comprises the work performed on two different setups at the same location, hereafter known as setup 1 and 2, respectively. Both are part of a long-term PV monitoring campaign and operate on similar types of experimental setup design.

The first setup consists of several poly-crystalline silicon (poly c-Si) modules mounted on a monitoring rack with 39° tilt of array. In this analysis, two similar modules labelled as ST422 and ST423, manufactured in the same batch by Suntech and having the exact same module parameters, are used for the evaluation of temperature coefficients. The module parameters are presented in (Paudyal and Imenes, 2019) and datasheet temperature coefficients are shown in Table (5). The irradiance in the plane of array is measured with a Kipp and Zonen CMP6 pyranometer last calibrated in 2017. The modules are monitored for their I-V characteristics every minute, while between I-V sweeps modules are kept at their individual maximum power point (MPP) (Imenes et al., 2011).

The second setup consists of PV modules enlisted in Table 2, mounted in a monitoring rack with 45° tilt of array. This setup has an extensive measurement facility that includes broadband and spectral irradiance measured in the horizontal plane (GHI), in the plane of array (GPOA), and at direct normal (DNI) conditions. Additionally, measured environmental parameters include ambient and module temperatures, wind direction and speed, atmospheric pressure, and relative humidity. The GHI, GPOA and DNI irradiances are measured with CMP11 pyranometers and a SHP1 pyrheliometer from Kipp and Zonen, while the spectral irradiances in the respective planes are measured by SolSIM-G and SolSIM-D2 spectroradiometers from Spectrafy Inc. (see Figs. 1 and 2).

Similar to setup 1, the PV modules in setup 2 are monitored for their I-V characteristics and kept at MPP between sweeps. The I-V measurements are recorded every 20 s, and the higher number of I-V sweeps provide a more detailed distribution of module parameters with varying environmental parameters. The recorded environmental parameter values are an average of sample values within one minute, and for the consistency between environmental and PV electrical data in the final analysis, the I-V parameters are also averaged to minute values.

Since only setup 2 is equipped with spectral irradiance measurement facilities, different spectral indices are used to account for spectral impact in the two setups. In setup 1, the spectral impact on PV modules is quantified using the spectral factor *SF*, which is calculated from Eq. 10. For setup 2, the availability of spectral irradiance measurements at POA conditions has been used to quantify the spectral indices APE and UF. The distribution of APE is used to express the typical spectral condition in the location while the UF is used for spectral correction of PV module parameters, i.e. I_{SC} and P_{MAX}.

Each PV module is equipped with a temperature sensor mounted on the back side of the module, directly behind a cell in the centre, to monitor the variation in the module temperature. Setup 1 employs Pt100 temperature sensors whereas setup 2 uses 110PV surface mount thermistors from Campbell Scientific. Overall, the guidelines prescribed in IEC 61724–1 have been followed for precise monitoring of PV performance (IEC, 2017). The class-A pyranometers with regular calibration intervals of two years have been installed. The recommendation for

Table 2
PV module parameters from experimental setup 2.

Module technology	Model No.	Datasheet values							
		I_{SC}	I_{MP}	V_{OC}	V_{MP}	P_{MAX}	(α)	(β)	(γ)
		[A]	[A]	[V]	[V]	[W]	[%/°C]	[%/°C]	[%/°C]
Mono c-Si [IBC Mono]	MonoSol 315VL5	10.02	9.53	40.5	33.1	315	0.06	−0.28	-0.38
HIT [Panasonic]	VBHN325SJ47	6.03	5.65	69.6	57.6	325	0.03	−0.25	−0.29
Poly c-Si [IBC Poly]	PolySol 270CS4	9.08	8.5	38.9	31.7	270	0.041	−0.31	−0.411
CIGS [Solibro]	SL2-FGen1.5	1.69	1.56	97.6	76.9	120	0	−0.29	−0.38

Fig. 1. Experimental setup 1 containing the poly c-Si PV modules used in this study. The full experimental details are described in (Paudyal and Imenes, 2019).

Fig. 2. Experimental setup 2 with PV modules from various technologies evaluated in this study.

current, voltage and power measurements have also been carefully followed. The temperature sensors and their positioning (both ambient and module) have also been with respect to the guidelines in (IEC, 2017; Paudyal et al., 2018). Generally cold climatic conditions together with a high share of diffuse irradiance is reported for this location (Imenes and Sclj, 2017). PV modules are thus not exposed to as high operating temperatures as locations closer to the equator, which is generally known to accelerate degradation processes. However, the modules can experience significant stress caused by thermal cycling, high precipitation and frequent freezing/thawing conditions.

3.2. Data preparation and correction

Data preparation and filtering is the most important and at times most underrated task in PV performance studies (Jordan and Kurtz, 2014). Both experimental setups record the I-V curves in a text file for each day, which are appended to form a dataframe. PV parameters and environmental parameters in experimental setup 1 are recorded in a single file whereas in setup 2, separate files for environmental parameters, spectral irradiance and PV data are recorded and matched in timestamps before being stored in a local database. Data consistency is ensured by common standard database routines, whereas data cleaning has to be performed in additional separate steps, either manually or by some automated filtering routine.

To closely replicate the conditions explained in IEC 60891, the PV

parameters are corrected to the STC irradiance value of 1000 Wm^{-2} and spectral corrections are applied. For setup 1, the spectral corrections are applied to P_{MAX} only (Eq. 10), since spectral correction for I_{SC} would mean self-referencing to the initial value. For setup 2, the spectral corrections are performed for both I_{SC} and P_{MAX}. Using the relations given in subSection 2.2, the PV parameters are corrected to STC conditions except for temperature (Mitterhofer et al., 2019).

Initially, the module parameters are filtered within reasonable set limits as denoted in Table 3. Additionally, to detect outliers, the ratio of short circuit current to POA irradiance (I_{SC}/G) was computed. As the histogram showed a normal distribution of the data, data-points outside two standard deviations from the mean ($\mu \pm 2\sigma$) were regarded as outliers and were subsequently removed. As the short circuit current is directly proportional to the irradiance, any potential shading of either sensor or PV module could be detected through this routine.

After initial screening, the data for each parameter is visually inspected for any remaining outliers. The visual inspection is first performed on STC irradiance corrected data, and secondly on the additional spectral corrected values. From the STC irradiance corrected P_{MAX} values in Fig. 3, the group of points enclosed by the red rectangle were identified as possible outliers. These data-points corresponded to periods with snow cover on the PV modules, which was verified from Fig. 4 obtained through an inspection camera installed on the monitoring site. As the CMP6 pyranometer is not ventilated, simultaneous snow cover on the irradiance sensor is a possible reason for these outliers not being removed by the standard deviation filtering routine for (I_{SC}/G).

Varying spectral conditions over the outdoor exposure period will impact the PV parameters to a certain degree. It is thus logical that quantifying spectral variation will provide a better correction for the PV parameters, i.e, I_{SC} and P_{MAX} as mentioned before. This is visible when comparing Fig. 5 with 6. The STC irradiance correction is seen to have a large spread of data especially in the 20–30 °C range. When applying the additional spectral corrections, the data are seen to follow an improved linear fit with less dispersion. The correlation coefficient improved from −0.89 (ST422) and −0.90 (ST423) to −0.97 for both modules. Interestingly, a detail hidden in Fig. 5 has been revealed in Fig. 6 as the group of data points contained in the black rectangle correspond to a limited time period of uncharacteristic external influences when modules were re-installed on the monitoring rack after transport to a certified laboratory for standard indoor characterisation.

Table 3
Initial screening limits of PV parameter values.

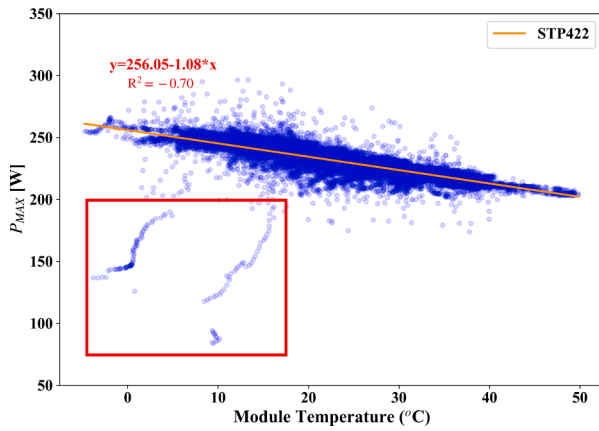| Parameters	Filtering range
G (POA)	> 400 Wm^{-2}
T (module)	−10 to 70°C
I_{SC}	0 to 15 A
V_{OC}	0 to 50 V
P_{MAX}	> 10 W

Fig. 3. STC irradiance corrected P_{MAX} values for module ST422 in setup 1 in 2016.

Fig. 4. Image captured by the inspection camera of a snow event in 2016 covering the PV modules (setup 1).
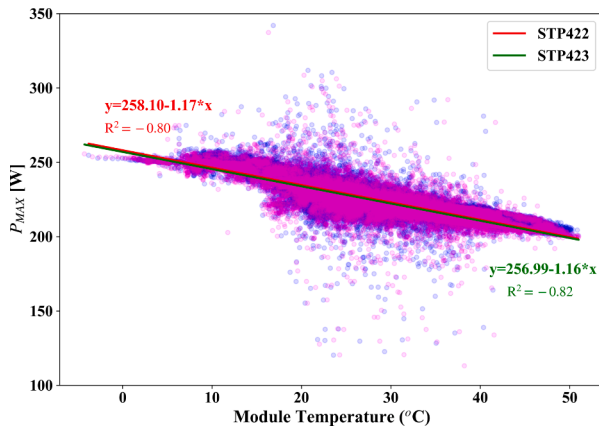

Fig. 5. Temperature coefficient calculation of P_{MAX} with STC irradiance correction for both modules in setup 1.

Fig. 6. Temperature coefficient calculation of P_{MAX} with STC irradiance and spectral correction for both modules in setup 1.

Fig. 7. The distribution of monthly averages of irradiance and temperature in experimental setup 1, over the time period 2013–2020.

Fig. 8. The distribution of monthly averages of environmental parameters in experimental setup 2, over the time period January 2020 to December 2020 (module temperatures only since April 2020).

4. Results and discussion

4.1. Irradiance and temperature distributions

The distribution of environmental parameters for experimental setup 1 is presented in Fig. 7. The POA irradiation, ambient temperature, and module temperature values are presented as monthly average values over the studied period from 2013 to 2020.

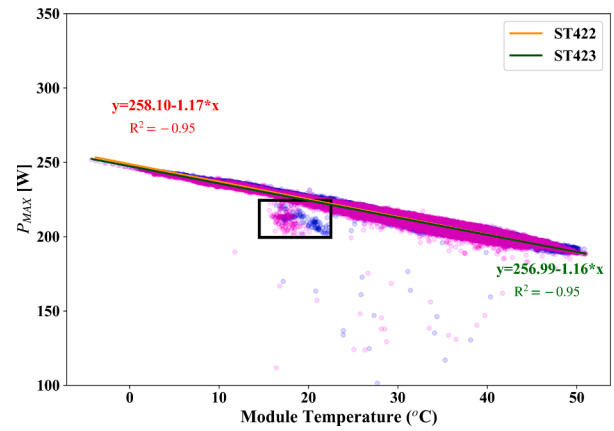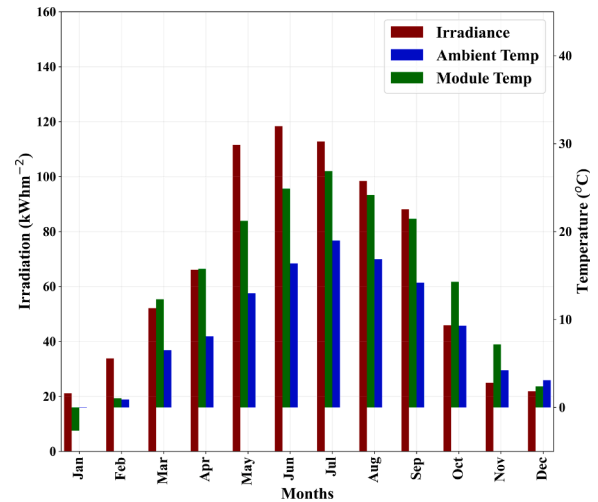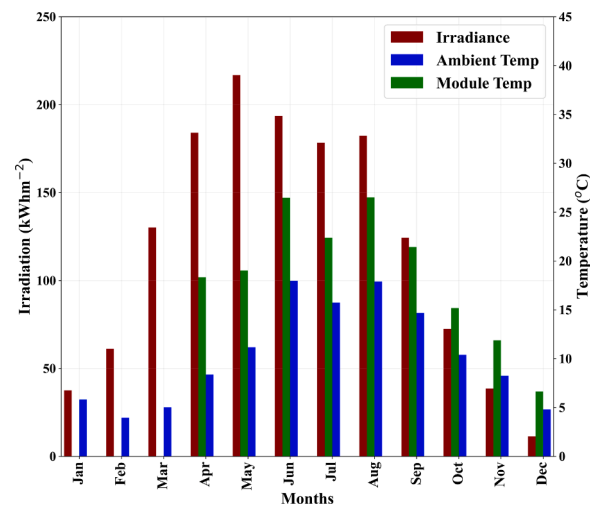Similarly, the distribution of environmental parameters for experimental setup 2 is presented in Fig. 8. The POA irradiation and ambient temperature values consist of monthly averages from January 2020 to

December 2020, while the monthly average module temperatures are available for 9 months only as the modules were fully instrumented for monitoring since April 2020.

As seen from Figs. 7 and 8, the distribution of irradiation at the plane of array of the two setups is not similar. Some difference is expected, but the data from setup 2 is considerably higher than the historical averages from 2013–2020 in setup 1. The readings from both setups for the same period (2020 January - 2020 December) was tested and it was seen that the difference of monthly averaged irradiation in the months of April, May and June gradually increase up to 65 kWhm^{-2}, while for other months the difference is below 10 kWhm^{-2}. This variation in irradiance was observed using the reference cells mounted in the corresponding plane of arrays in the two setups, as presented in Fig. 9. There can be various reasons for this difference, as setup 1 has a CMP6 pyranometer in 39° POA tilt while setup 2 has a CMP11 pyranometer in 45° POA tilt. However, a more significant influence is likely caused by reflected light from the ground (albedo) or surrounding objects. A 40 kW grid-connected system with modules at 10° tilt in an east–west configuration is installed in front of the PV rack in setup 2, which could introduce non-uniform albedo effects on the measured irradiance. The exact reason for this variation is under investigation and is thus not yet confirmed.

Regarding the ambient temperature, the difference between the two setups is less than 1 °C. The displayed module temperatures in both of Figs. 7 and 8 refer to the poly c-Si modules. As module temperature can vary depending on the position in the rack, thermophysical properties (Theristis et al., 2018), and the accuracy of temperature sensors, the difference of 2 °C between module temperatures is within the normal expected range.

4.2. Spectral distribution

The distribution of spectral variation in the experimental location is presented in terms of APE whereas the impact of spectral variation for applicable PV parameters is quantified with SF and UF. The distribution of APE for the period of full data availability in setup 2 (May 1, 2020 to December 31, 2020) in the present analysis is presented in Fig. 10. Also the distribution of APE values for a full year (from 1st January 2020 to 31st December 2020) is presented in the inset of the same figure.

As the APE value for the standard AM1.5 reference spectrum is 1.59 eV, referring to the 350–1700 nm range, the mean APE value of 1.62 eV indicates a generally blue-shifted spectrum on average during the one year period. Evaluating the experimental period May-December only, the mean APE value of 1.65 eV signifies an even stronger blue shift of the incident spectra, which is expected as the period incorporates the
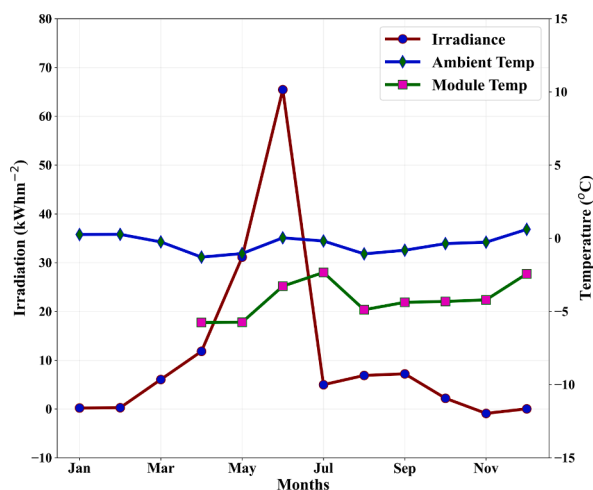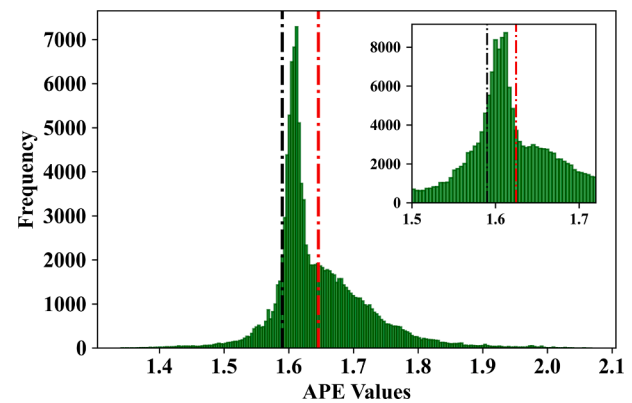

Fig. 10. The average distribution of APE (350–1700 nm range) for the experimental period May-December 2020 in setup 2. APE distribution for a full year (2020) is presented in the inset. The black dotted line represents the APE value for reference AM1.5G spectrum whereas red dotted line represents the mean APE value for period under consideration.

summer months in the northern hemisphere.

Typical SR curves representing various PV technologies is presented in Fig. 11. From the SR curves, it can be noticed that the maximum absorption of c-Si corresponds to the near-infrared region of the spectrum. Also, the technologies with higher bandgap energies, i.e. a-Si and CdTe, have a narrower SR-range compared to CIGS and conventional c-Si. HIT is not presented in the figure but has a similar curve to CIGS and c-Si technologies (Louwen et al., 2017). The SR-curve absorption limit for a-Si and CdTe are closer to the visible region limit compared to other module technologies and the narrow SR curve of these module technologies encompasses the highest intensity part of the incident spectrum. These technologies are therefore more susceptible to spectral variation. Higher energy content in the blue-rich region is beneficial to these PV module technologies, whereas for CIGS, HIT and conventional c-Si modules, spectra with higher energy content in the near infrared region is advantageous. Thus, the blue shift of the spectrum during summer period, also verified through the measured APE values in setup 2, incurs spectral losses for technologies with wider SR- range, including crystalline silicon devices.

The distribution of SF for the experimental period of 2013–2020 from setup 1 is presented as box plot in Fig. 12. In the box plot, the ends of boxes represent the first and third quartile of the data whereas the horizontal line within the box represents the median of the data. The error bars represent the minimum and maximum values, and the outliers are discarded. As seen from the figure, the SF is less than 1 during the

Fig. 9. Difference (setup 2 - setup 1) between irradiance and temperature parameters measured in the two setups during the full year of 2020.
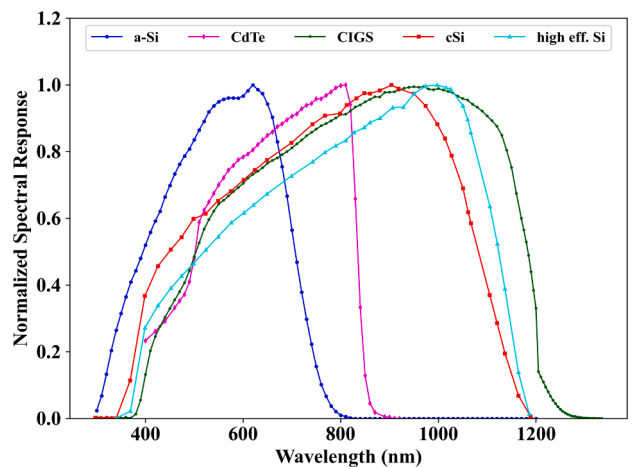

Fig. 11. Typical (normalized) spectral response curve of various PV technologies. [Source: Fraunhofer ISE].
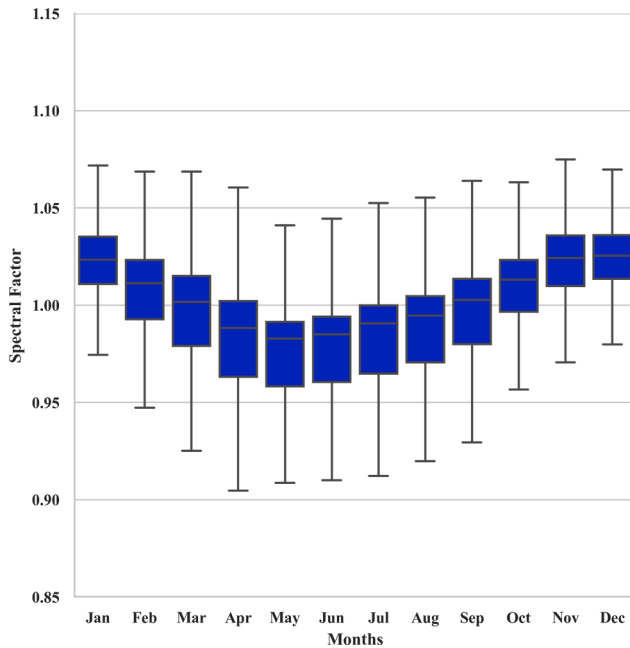
Fig. 12. The distribution of SF for the poly c-Si modules in experimental setup 1, based on irradiance data from 2013 to 2020.

summer period, which indicates a blue shift of the spectra due to higher energy content of the blue wavelength region of spectrum during the months of highest irradiance conditions relative to the standard spectrum. In winter, the opposite effect is seen with SF values above 1 and red-shifted spectra. SF values above 1 represent higher short circuit current produced by PV device under the actual solar spectral distribution compared to that generated under the standard solar spectrum AM 1.5G, when considering spectral aspects only and conversely is true for SF values less than 1.

Similar to the APE, the distribution of UF values for the duration of the experimental period are presented in Fig. 13, with the inset showing the distribution for one full year (2020). The UF values for the three PV technologies c-Si, CIGS and HIT are slightly higher than their respective AM1.5G reference values, denoting a higher energy content received within the active SR region of the aforementioned technologies. As a UF value larger than the AM1.5G reference spectrum is referred to as a blue-rich spectrum, a general blue-shift of the spectrum at the present location is evident from both the yearly and the experimental duration.

4.3. Analysis of annual temperature coefficients in setup 1

The values of α, β, and γ for two poly c-Si modules investigated in setup 1 were first calculated from the long-term dataset (8 years of data, filtered above 400 Wm^{-2}) and are presented in Table 4.

From Table 4, a significant difference between the datasheet values and calculated values of α and β is seen, whereas γ is found to be relatively close to the manufacturer's specification. This difference between datasheet values and measured values is gradually reduced when the irradiance range used for filtering is steadily increased in steps of 100 Wm^{-2}. Applying the most strict filtering to the near-STC range (990 Wm^{-2} to 1010 Wm^{-2}) improved the α, β and γ estimation and the temperature coefficients were found to be similar to the datasheet values as shown in Fig. 14.

Additionally, the development of temperature coefficients for each year from 2013 to 2020 are provided in Table 5. It is important to mention that temporary malfunction of temperature sensor of module ST423 was found during some periods of 2015 and the corresponding data have been removed from the subsequent analysis. Although the datasets are filtered ($> 400 W m^{-2}$) to reduce the impact of spectral
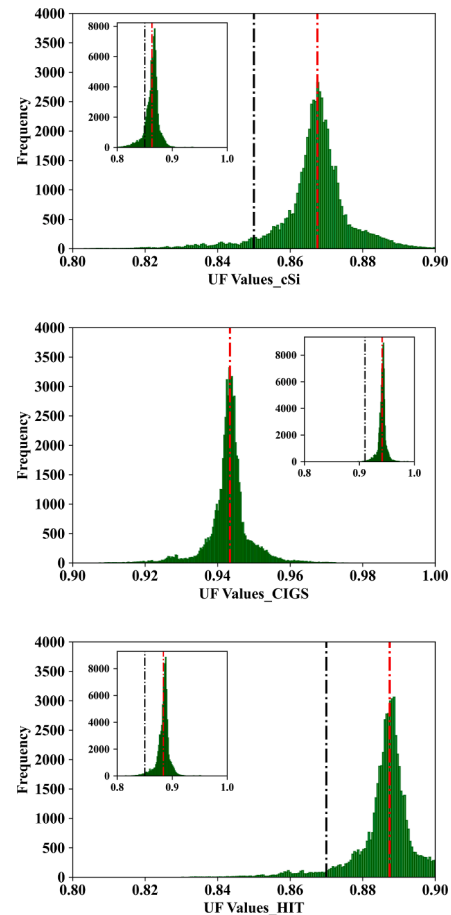

Fig. 13. The average distribution of UF for 3 PV technologies, c-Si, CIGS and HIT, for the experimental period in setup 2. Respective yearly UF distributions are presented in the inset. The black dotted line represents the APE value for reference AM1.5G spectrum whereas red dotted line represents the mean APE value for period under consideration.

Table 4

Temperature coefficients for two c-Si modules (ST422 and ST 423), calculated directly from the total dataset ($> 400 W m^{-2}$) where spectral corrections are applied on P_{MAX} only.

Parameters	Datasheet value [%/$^\circ C$]	Calculated value (ST422) [%/$^\circ C$]	Calculated value (ST423) [%/$^\circ C$]
α	0.045	0.085	0.061
β	-0.34	-0.25	-0.25
γ	-0.47	−0.51	−0.49

variations (Silverman et al., 2014), a shift to the blue region of the spectrum is seen in the summer from the measured spectral data in setup 2. As the experimental site lies in a high latitude coastal location it experiences higher air mass values on average, and the presence of higher water content in the atmosphere around coastal regions are known to influence the spectral attenuation. In such locations spectral shifts to red and blue rich regions may not be equally distributed throughout the year, with a higher share of cloudy sky conditions in the winter.

The benefit of using spectral correction is visible from Fig. 15. Here, the two bars for each year represent irradiance correction only and additionally spectral corrected γ values of the ST422 c-Si module. Error bars are included to represent the variance. As the figure shows narrowing of variance from the additional use of spectral correction, it can be concluded that correcting for variation in spectrum can improve the estimation of the temperature coefficient of P_{MAX}. Due to the possibility
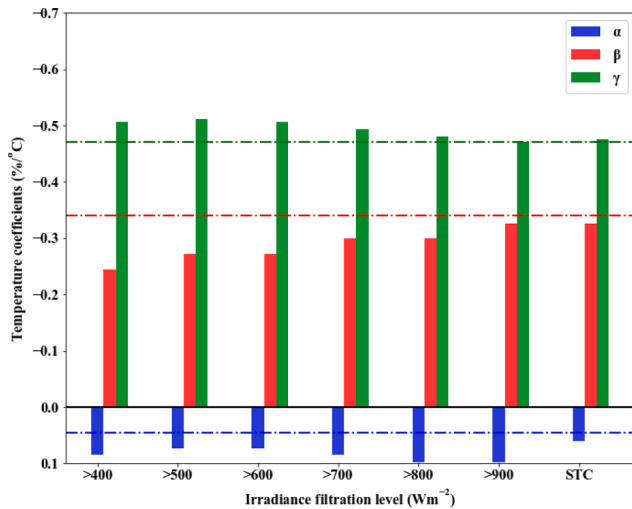
Fig. 14. Temperature coefficients of ST422 module calculated from various irradiance filters labelled in x-axis. The dotted lines denote the datasheet value for each temperature coefficient.

of in-homogeneous temperature and irradiance distributions across the module surface, thermal lag and natural weather fluctuations it can be very difficult to get completely correlating results using outdoor measurements compared to controlled indoor measurements.

Overall, a difference is apparent between the datasheet and measured values while employing a general filtering limit of $400 Wm^{-2}$. The temperature coefficients of I_{SC} and V_{OC} have larger differences from the datasheet values than the P_{MAX} coefficient. As evident in the Figs. 3 and 5, most of the data are dispersed within module temperatures of 15–35 °C, meaning the slope of the regression line through these datasets will be influenced by this dispersion. Furthermore, low solar elevation angles during winter months can introduce non-uniform albedo effects on the irradiance sensor and PV modules even when installed in the same mounting rack. This in turn can introduce additional dispersion of data when module parameters are corrected to STC irradiance, which propagate to the linear regression plot used to determine the temperature coefficients. In addition, the α values are not as strongly correlated to the temperature variations compared to β, and γ values, so, the linear regression through dispersion of such data can also sometimes cause the α values to be negative.

Additional verification of the temperature coefficients were done through a field test on a clear autumn day with stable irradiance conditions (18th September 2020, test setup 1) following the IEC 60891 specifications. Calculating the α, β, and γ coefficients for poly c-Si module ST423 resulted in the values 0.146 %/°C, −0.36 %/°C, and −0.45 %/°C, respectively. From the comparison between measured and datasheet values, very good agreement is found between temperature coefficients of V_{OC} and P_{MAX} but a high difference is seen for the I_{SC}

coefficient. Such difference between datasheet values and calculated values using equations are reported elsewhere too (Mahmood et al., 2017; Osterwald et al., 2015; Mihaylov et al., 2014). As α is a strong function of spectral irradiance, the higher measured α values compared with the datasheet value can be related to spectral impact since this measurement was carried out in AM 1.9 conditions (the lowest available AM condition for the day 18 September). In this setup spectral correction was applied to P_{MAX} only, therefore the spectral effect is assumed to have played a role in the difference seen for the I_{SC} temperature coefficient. Spectral correction of P_{MAX} has yielded results consistently closer to the datasheet values compared to the STC irradiance only corrected datasets. Hence, additional spectral correction is required to calculate the temperature coefficient of I_{SC}.

In case of V_{OC}, the temperature coefficient estimation is seen to significantly improve with a narrower filtering range as the limit moves closer to the STC irradiance value. However, the STC correction of V_{OC} has been performed considering the diode ideality factor as 1, which can cause misrepresentation of the actual results. To investigate the potential impact of altering the ideality factor, the experimental data gathered from 18th September 2020 following the IEC 60891 standard were corrected to STC values using the typical range of ideality factor between 1 and 2, as shown in Fig. 16. The STC correction was applied with Eq. 12. It is seen that the temperature coefficient for V_{OC} also varies with the ideality factor alone, but it has only a small influence (-0.369 %/°C for m = 1 and −0.377 %/°C for m = 2). Thus the assumption of $m = 1$ as in this work seems fair.

The difference between temperature coefficients extracted from long term I-V data and the values from direct measurement on a clear day
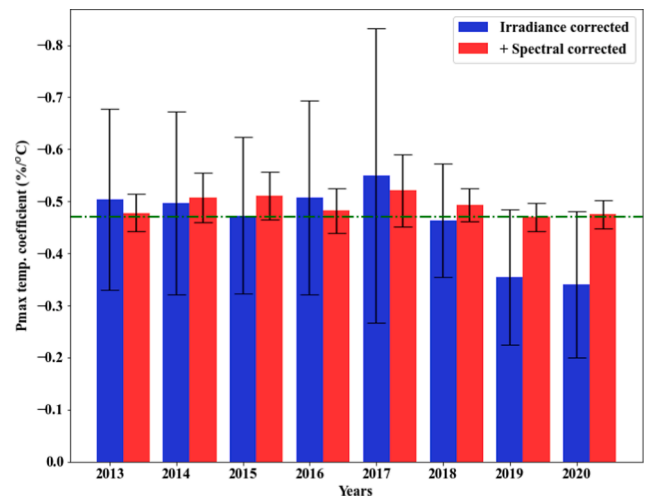

Fig. 15. Irradiance corrected only and additionally spectral corrected temperature coefficient values for P_{MAX}. The datasheet value for γ is represented by a green dotted line.

Table 5
Temperature coefficient of two poly c-Si modules in setup 1, after STC irradiance correction only and with additional spectral correction.

Years	Datasheet values			STC Irradiance Corrected						Spectral corrected					
	(α)	(β)	(γ)	$(\alpha)[\%/°C]$		$(\beta)[\%/°C]$		$(\gamma)[\%/°C]$		$(\alpha)[\%/°C]$		$(\beta)[\%/°C]$		$(\gamma)[\%/°C]$	
	$[\%/°C]$	$[\%/°C]$	$[\%/°C]$	ST422	ST423	ST422	ST423	ST422	ST423	ST422	ST423	ST422	ST423	ST422	ST4223
2013	0.045	−0.34	−0.47	−0.003	−0.012	−0.24	−0.23	−0.50	−0.52	-	-	-	-	−0.48	-0.49
2014	0.045	−0.34	−0.47	0.040	0.028	−0.25	−0.24	−0.50	−0.49	-	-	-	-	−0.51	-0.49
2015	0.045	−0.34	−0.47	0.063	0.030	−0.25	−0.22	−0.47	−0.51	-	-	-	-	−0.51	-0.48
2016	0.045	−0.34	−0.47	−0.005	−0.013	−0.25	−0.24	−0.51	−0.52	-	-	-	-	−0.48	-0.48
2017	0.045	−0.34	−0.47	−0.007	−0.017	−0.24	−0.22	−0.54	−0.53	-	-	-	-	−0.52	-0.50
2018	0.045	−0.34	−0.47	0.051	0.040	−0.27	−0.25	−0.46	−0.46	-	-	-	-	−0.49	-0.48
2019	0.045	−0.34	−0.47	0.144	0.135	−0.25	−0.24	−0.35	−0.42	-	-	-	-	−0.47	-0.50
2020	0.045	−0.34	−0.47	0.171	0.164	−0.23	−0.24	−0.33	−0.39	-	-	-	-	−0.47	-0.51
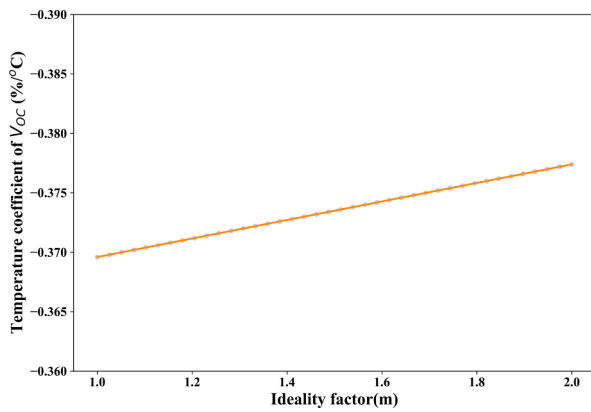
Fig. 16. Temperature coefficient of V_{OC} calculated from values of ideality factor ranging between 1 and 2.

Table 6
Calculation of temperature coefficients of electrical parameters for module ST422 (setup 1), based on irradiance-corrected values of I_{SC} and V_{OC} and additionally spectral-corrected P_{MAX} values. *FF* is calculated from these parameters.

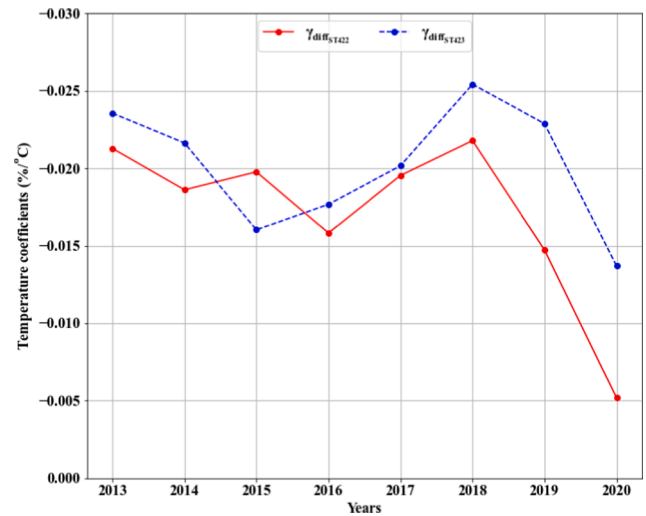| Years	Datasheet values			Temperature coefficients from measurements			
	(α)	(β)	(γ)	(α)	(β)	(γ)	(κ)
	$[\%/^{\circ}C]$	$[\%/^{\circ}C]$	$[\%/^{\circ}C]$	$[\%/^{\circ}C]$	$[\%/^{\circ}C]$	$[\%/^{\circ}C]$	$[\%/^{\circ}C]$
2013	0.045	−0.34	−0.47	−0.003	−0.24	−0.48	−0.25
2014	0.045	−0.34	−0.47	0.040	−0.25	−0.51	−0.32
2015	0.045	−0.34	−0.47	0.063	−0.25	−0.51	−0.34
2016	0.045	−0.34	−0.47	−0.005	−0.25	−0.48	−0.25
2017	0.045	−0.34	−0.47	−0.007	−0.24	−0.52	−0.29
2018	0.045	−0.34	−0.47	0.051	−0.27	−0.49	−0.30
2019	0.045	−0.34	−0.47	0.144	−0.25	−0.47	−0.39
2020	0.045	−0.34	−0.47	0.171	−0.23	−0.47	−0.42

Fig. 17. Comparison of the difference in γ coefficients calculated from linear regression versus using Eq. 3 (with values from table 6), for modules ST422 and ST423.

(following the IEC 60891 standard) is considerable. Attempting to explain this difference, in case of I_{SC} the long term data consists of data points representing a larger variation in spectral conditions, which ultimately tame the spectral gains/losses to a smaller magnitude compared to the one encountered on 18th September. It was possible to observe relatively stable irradiance (varying from 776 Wm^{-2} to 741 Wm^{-2} in POA) and a module temperature range of 23°C to 37°C during the direct measurement. For V_{OC}, these conditions provided a near perfect linear fit of the data points ($R^2 = 0.99$), which in turn contributed to a β value close to the datasheet value. Similarly, the spectral corrected data for P_{MAX} from direct measurement on 18th September 2020 resulted in a temperature coefficient value γ in close proximity of the datasheet value.

Theoretically, the temperature coefficients are not expected to change unless degradation mechanisms affect the optical or electrical material properties. Prolonged exposure in outdoor conditions with humidity, UV light, infiltration of ions triggering corrosion or chemical reactions and an increment in the series resistance within the module can change the temperature coefficients (Mahmood et al., 2017). Mechanical stress caused by wind and snow loads can induce or accelerate crack formation in the PV cells, affecting current collection and fill factor. Field aged modules can undergo browning and discoloration of the lamination, which can degrade the spectral response compared to the initial SR values (Pern et al., 1991). The temperature of the cells affected by these degradation modes can also be higher compared to the normally operating cells. In an earlier study, analysis of electrical parameters of the same modules as evaluated here did not show any signs of visible degradation (Paudyal and Imenes, 2019), and hence the SR is assumed to have remained unchanged.

The above discussion highlights the usefulness of long term filtered data to evaluate temperature coefficient values. It should be noted that the number of data points available from each year may differ and unavailability of data for a particular month/season could introduce uncertainties in the temperature coefficients calculated from measurements. For instance, unavailability of data during periods with high air-mass can bias the data to spectral gain conditions. This could also be the source of deviation for α and γ in this analysis, as setup 1 was affected by regular downtime of the data acquisition system. In contrast, small year-on-year variation of β values are seen despite the data size being different, indicating its strong dependence on temperature.

In addition to the aforementioned parameters, the temperature coefficient of *FF* was also calculated to verify the relation given in Eq. 3. The results from the computation of all coefficients are presented in Table 6. The temperature coefficient κ was calculated from a linear regression plot of *FF* versus module temperature. Fig. 17 is presented to show the difference between temperature coefficients of P_{MAX} calculated from the linear regression versus the sum of α, β and κ coefficients from

Eq. 3. As the figure shows, the difference between the two results is small and the relation of temperature coefficients defined in Eq. 3 was thus verified within acceptable accuracy.

4.4. Monthly distribution of temperature coefficients in setup 1

The distribution of monthly average temperature coefficients based on eight years of data in setup 1 is presented in Fig. 18.

The I_{SC} temperature coefficient does not seem to follow any particular pattern, with random variation of values distributed throughout the year. Values are consistently higher than the datasheet values for both the modules. For β and γ, the values are relatively constant over the months. The uncertainty is higher during the winter months due to generally lower irradiance conditions and correspondingly low number of data points. Also, the extended temperature range in the summer improves the linear regression fit with reduced uncertainty of the temperature coefficient estimation.

4.5. Mann Kendall trend results for setup 1

The MK test for determination of trends in the monthly, seasonal and yearly values of temperature coefficients are carried out using the *pyMannKendall* module in python (Hussain and Mahmud, 2019). The yearly values of α, β, and γ were tested for the presence of increasing or decreasing trend. The results of the tests are presented in Table 7. The
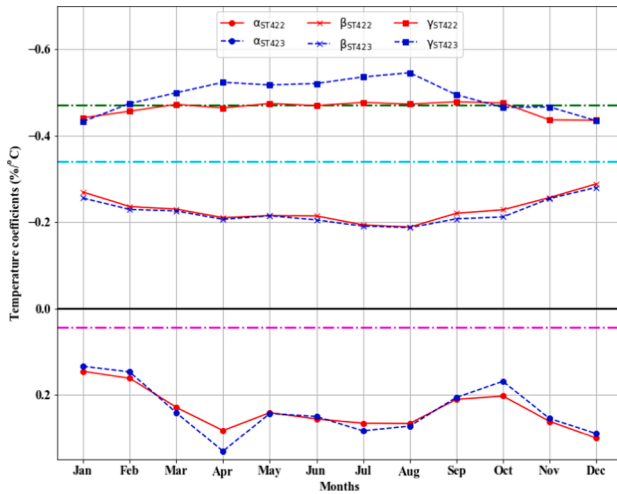
Fig. 18. Monthly distribution of temperature coefficients of I_{SC} (top), V_{OC} (middle) and P_{MAX} (bottom). The magenta, cyan and green lines denote the datasheet values for α, β and γ, respectively. (Values are based on irradiance-correction of I_{SC} and V_{OC} and additional spectral correction of P_{MAX}.)

months considered in this test are the two extreme months for the temperature and irradiance distributions. June and December are characterised with the highest and lowest amount of irradiance, thus the PV parameters can be assessed on the relation of irradiance versus temperature in the case of these extreme months. The results from both poly c-Si modules in setup 1 for α, β, and γ showed P values higher than 0.05 supporting the null hypothesis, which means absence of any kind of monotonic trend. Thus the results show no presence of trend for any of the temperature coefficients for both modules tested.

The development of temperature coefficients were also tested on a seasonal basis for the four seasons, namely winter, spring, summer and autumn. Again, there is no statistical evidence of presence of any significant trend. A trend of increasing β whereas decreasing α and γ is visible for ST423 module in the winter season. As discussed earlier this could be the influence of higher uncertainty in temperature coefficient determination rather than an underlying phenomenon as no trend is visible in other cases. The study of statistical variance showed the least dispersion of all temperature coefficient values (α, β, and γ) during spring compared to other seasons. Finally, the yearly analysis also showed the absence of monotonic trend for any of the coefficients. This gives rise to the understanding of temperature coefficients for c-Si modules operating under conditions similar to this location, where all three parameters considered do not significantly change over the tested 8-year period of

outdoor exposure.

4.6. Analysis of temperature coefficients in setup 2

The temperature coefficients for the PV modules in setup 2 is given in Table 8. It was seen from the analysis of setup 1 that the stricter irradiance range filtering and spectral corrections can provide a good estimation of temperature coefficients. Therefore, a similar stricter filtering range, i.e., POA irradiance between 900 Wm^{-2} and 1100 Wm^{-2}, is chosen for the analysis. In addition to the analysis done in setup 1, the I_{SC} is corrected for spectral irradiance variations using the UF, while P_{MAX} is corrected using both UF and SF to compare the correction by each metric.

The results display a close match between the datasheet values and measurement-based values of temperature coefficients for I_{SC}, V_{OC} and P_{MAX}. The measured β values are almost identical to the datasheet value. Also, as seen in Fig. 19, the spectral correction using UF improved the α values compared to the irradiance-only corrected values. Meanwhile, the γ values estimated by using SF were seen to be closer to the datasheet value than the coefficients calculated using UF, as seen in Fig. 20.

Despite being the PV device dependent index, the spectral correction using UF (as compared to SF) did not improve the coefficient estimation as expected. A possible explanation is that the real SR data for modules in setup 2 was not available and the UF was calculated from the standard SR range for each technology available from the literature (see Fig. 11), which could have caused some mismatch. It is seen that the SF is here a better equipped index for spectral correction compared to UF, as the SF couples the spectral irradiation variation to the SR of individual PV devices.

All results from setup 1 and 2 have been compared with the temperature coefficient values provided by the manufacturers of the given module technologies. As these datasheet values also have uncertainties related to the manufacturing tolerances and instrumentation accuracies, a comparison with indoor laboratory standard measurement performed before and after outdoor exposure would be an interesting addition to support the long-term evaluation of temperature coefficients.

5. Conclusions

The temperature coefficients of I_{SC}, V_{OC} and P_{MAX}, i.e., α, β and γ, have been calculated from outdoor field measurements of several PV modules in two experimental setups with different instrumentation. The long term development of the temperature coefficients of poly c-Si modules were investigated in setup 1 based on eight years of outdoor exposure. The impact of spectral correction using both spectral factor and useful fraction was investigated in setup 2, consisting of a more

Table 7
Mann Kendall test statistics for poly c-Si modules in setup 1.

Modules	Series	$(\alpha)[\%/^\circ C]$				$(\beta)[\%/^\circ C]$				$(\gamma)[\%/^\circ C]$			
		P	Z	Slope	Trend	P	Z	Slope	Trend	P	Z	Slope	Trend
ST422	June	1.00	0.00	0.00	N	1.00	0.00	−0.00	N	0.072	1.80	0.03	N
	December	0.17	−1.36	−0.001	N	0.39	0.87	0.001	N	1.00	0.00	0.00	N
	Winter	0.12	−1.6	−0.02	N	0.60	0.52	0.006	N	0.47	−0.73	−0.02	N
	Spring	0.46	0.74	0.01	N	0.801	−0.25	−0.004	N	0.81	0.25	0.012	N
	Summer	0.54	-0.62	−0.003	N	0.54	0.62	0.002	N	0.39	−0.87	−0.01	N
	Autumn	0.06	1.86	0.02	N	0.39	0.87	0.003	N	0.26	1.11	0.02	N
	Annual	0.17	1.36	0.02	N	0.57	0.62	0.001	N	0.54	0.62	0.003	N
ST423	June	0.13	1.50	0.001	N	0.71	−0.38	−0.003	N	0.71	0.38	0.004	N
	December	0.17	−1.36	−0.002	N	0.064	1.86	0.003	N	0.17	1.36	0.006	N
	Winter	0.04	-2.10	−0.04	Y/D	0.02	2.35	0.01	Y/I	0.02	−2.35	−0.04	Y/D
	Spring	0.22	1.23	0.02	N	1.00	0.00	−0.001	N	0.46	0.74	0.024	N
	Summer	0.27	1.11	0.01	N	0.90	−0.13	−0.00	N	0.27	1.11	0.01	N
	Autumn	0.06	1.86	0.01	N	0.71	0.37	0.001	N	0.17	1.36	0.01	N
	Annual	0.17	1.36	0.02	N	0.39	−0.87	−0.001	N	0.11	−1.61	−0.003	N

Test statistics: (P - p-value, Z - z-value, Slope (Y/N) - Yes/No, I/D (Increasing/Decreasing).

Table 8

Temperature coefficients of four different module technologies in setup 2: Datasheet values and outdoor calculated values after STC irradiance correction and UF spectral correction.

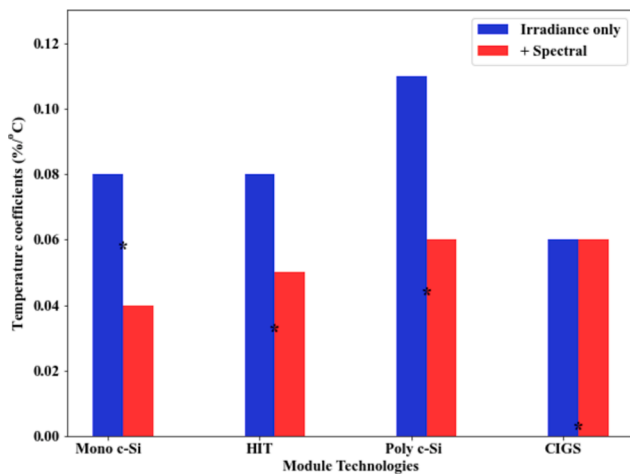| Module technologies	Datasheet values			STC irradiance corrected			UF corrected		
	(α)	(β)	(γ)	(α)	(β)	(γ)	(α)	(β)	(γ)
	[%/°C]	[%/°C]	[%/°C]	[%/°C]	[%/°C]	[%/°C]	[%/°C]	[%/°C]	[%/°C]
Mono c-Si	0.06	−0.28	−0.38	0.08	−0.27	−0.30	0.04	−0.27	−0.33
HIT	0.03	−0.25	−0.29	0.08	−0.24	−0.22	0.066	−0.24	−0.24
Poly c-Si	0.041	−0.31	−0.41	0.11	−0.28	−0.34	0.07	−0.28	−0.37
CIGS	0.0	−0.29	−0.38	0.06	−0.26	−0.26	0.06	−0.26	−0.29

Fig. 19. Temperature coefficients of I_{SC} obtained after irradiance and additional spectral correction using UF. The black asterisks on each technology denote the datasheet values.
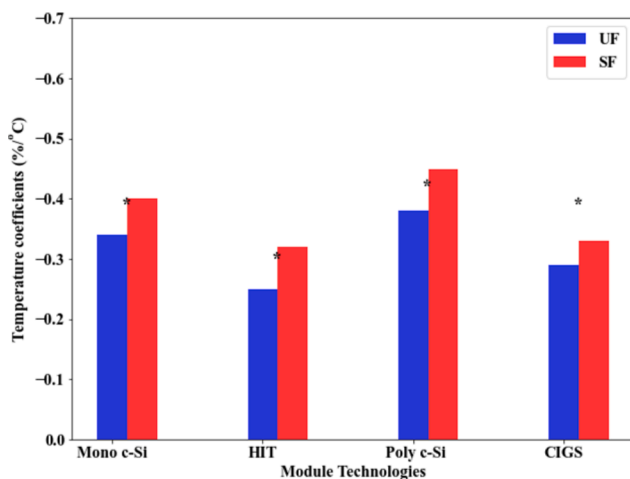

Fig. 20. Temperature coefficients of P_{MAX} obtained after spectral correction using UF and SF. The black asterisks on each technology denotes the datasheet value.

recent experimental facility with different PV technologies and spectral irradiance measurements.

In setup 1, applying spectral corrections to the STC irradiance corrected P_{MAX} values by means of the PV-specific spectral factor SF, yielded improved estimates of γ in close proximity to the datasheet value. More specifically, for the two analyzed poly c-Si modules the standard deviation of annual variation in γ values was reduced from 5.5 % and 7.5 % before spectral correction, to 1.2 % and 1.8 % after spectral correction. The corresponding range in values as compared with the datasheet

γ value was reduced from [+13, −17] % and [+15, −30] %, to [0, +11] % for both modules after spectral correction. Setting stricter irradiance filtering limits improved the estimation of β and γ, while α remained relatively unaffected. The shift towards datasheet values were noted for γ and β values, when the irradiance threshold was changed from 400 Wm^{-2} to 900 Wm^{-2}. While γ shifted from −0.51 %/°C to −0.47 %/°C, the β value changed from −0.25 %/°C to −0.33 %/°C after the irradiance threshold was modified. The datasheet values of γ and β were −0.47 %/°C and −0.34 %/°C, respectively. In comparison, similar stricter filtering ranges near the STC irradiance with additional spectral corrections in setup 2 improved the α coefficient as well.

Monthly average values of temperature coefficients were calculated over all eight years of data to analyse the seasonal and annual development, and no obvious pattern was found. Additionally, field test was performed to calculate the temperature coefficients of one module using IEC 60891 guidelines. The β and γ values of −0.36 %/°C, and −0.45 %/°C extracted respectively from the test, were found to have a good agreement to the datasheet value. A significant difference however, was seen for the I_{SC} coefficient as also reported in other literatures. Since α is closely associated with the spectral irradiance, the AM1.9 condition when the measurements were carried out, can be associated with the higher deviation from the datasheet value. The non-parametric Mann–Kendall test was used to evaluate possible degradation of the temperature coefficients. The results of the MK test obtained within a 95 % confidence interval showed that the values of α, β, and γ did not show a significantly varying trend over several years of outdoor exposure. Also, the development of trends in the temperature coefficients over time were analyzed for the extreme months of June and December and no significant trend was seen. The modules under test were examined for degradation in a separate study and were found to not have degraded. With the annual values of the temperature coefficients showing no monotonic trend, any year to year differences in temperature coefficients can be related to the data points available.

In setup 2, module temperature coefficients were calculated for the four module technologies mono c-Si, poly c-Si, HIT and CIGS. The average APE value of 1.62 eV for 350–1700 nm suggested a general blue shift of the spectrum, also verified by the UF values for c-Si, CIGS and HIT technologies. The useful fraction according to each individual PV technology was employed to correct for the variation in spectral distribution based on measured spectral irradiance for both I_{SC} and P_{MAX}. The α values for mono c-Si, HIT, poly c-Si and CIGS technologies were found as 0.04 %/°C, 0.05 %/°C, 0.06 %/°C and 0.06 %/°C compared to the datasheet values of 0.055 %/°C, 0.03 %/°C, 0.041 %/°C and 0.00 ± 0.04 %/°C respectively. This was a significant improvement compared to the only irradiance corrected values. Similarly, the performance of UF and SF were tested for the spectral correction of P_{MAX} data. The absolute difference between the datasheet values of γ values obtained for mono c-Si, HIT, poly c-Si and CIGS technologies from UF correction were 0.04 %/°C, 0.04 %/°C, 0.03 %/°C and 0.09 %/°C whereas, applying SF as a correction metric, the difference was found to be 0.02 %/°C, 0.03 %/°C, 0.04 %/°C and 0.05 %/°C respectively. Although indices like APE and UF are suitable for denoting the blue- or red-richness of the spectrum, the results in this study did not provide accurate estimation of the

subsequent spectral loss or gain by these factors. Thus, SF was found to be a better estimator of spectral impact on PV performance.

The results from both setups demonstrate that long term data can be used to determine the temperature coefficients of PV module parameters with satisfactory accuracy. While more stringent data filtering regimes need to be employed for better precision, some locations also need to take into consideration the remaining data size after filtering. For the high-latitude experimental site in this work, an initial irradiance limit filter of 400 Wm^{-2} was used to have enough data points from winter months. A larger error margin between measured and datasheet temperature coefficient values can be correlated with this irradiance limit filter, and accuracy was seen to improve with stricter filtering. In conclusion, the results emphasize the importance of considering spectral impacts on the determination of PV module parameters, even for PV devices with broad spectral response.Although the PV modules in this experimental study were found to have not degraded, longer exposure duration is more likely to introduce different forms of degradation in PV modules. With such longer exposure, the methods presented in this paper will be even more applicable to study the progression of temperature coefficients. As the degradation of temperature coefficients is not found in the present location, other similar studies from various climatic conditions are suggested for confirmation.

Declaration of Competing Interest

The authors declare that they have no known competing financial interests or personal relationships that could have appeared to influence the work reported in this paper.

References

Allet, J., Baumgartner, F., Sutterlueti, J., Schreier, L., Pezzotti, M., Haller, J., 2011. Evaluation of PV system performance of five different PV module technologies, in: 26thEuropean Photovoltaic Solar Energy Conference, pp. 3239–3247. doi:10.4229/26thEUPVSEC2011-4DO.6.2.

Alonso-Abella, M., Chenlo, F., Nofuentes, G., Torres-Ramírez, M.J.E., 2014. Analysis of spectral effects on the energy yield of different PV (photovoltaic) technologies: The case of four specific sites. Energy 67, 435–443. https://doi.org/10.1016/j.energy.2014.01.024.

Berthod, C., Strandberg, R., Yordanov, G.H., Beyer, H.G., Jan, O., 2016. On the variability of the temperature coefficients of mc-Si solar cells with irradiance. Energy Procedia 92, 2–9. https://doi.org/10.1016/j.egypro.2016.07.002.

Betts, T., Infield, D., Gottschalg, R., 2004. Spectral irradiance correction for pv system yield calculations. In: 19th Photovoltaic Solar Energy Conference.

Blain, G.C., 2015. The influence of nonlinear trends on the power of the trend-free pre-whitening approach. Acta Scientiarum. Agronomy 37, 21–28.

Dierauf, T., Growitz, A., Kurtz, S., Cruz, J.L.B., Riley, E., Hansen, C., 2013. Weather-Corrected Performance Ratio. Technical Report. NREL. doi:10.2172/1078057.

Dubey, R., Batra, P., Chattopadhyay, S., Kottantharayil, A., Arora, B.M., Narasimhan, K.L., Vasi, J., 2015. Measurement of temperature coefficient of photovoltaic modules in field and comparison with laboratory measurements. In: 2015 IEEE 42nd Photovoltaic Specialist Conference (PVSC), pp. 1–5.

Duck, B.C., Fell, C.J., Anderson, K.F., Sacchetta, C., Du, Y., Zhu, Y., 2018. Determining the value of cooling in photovoltaics for enhanced energy yield. Sol. Energy 159, 337–345. https://doi.org/10.1016/j.solener.2017.11.004.

Dupré, O., Vaillon, R., Green, M., 2015. Physics of the temperature coefficients of solar cells. Sol. Energy Mater. Sol. Cells 140, 92–100. https://doi.org/10.1016/j.solmat.2015.03.025.

Eke, R., Betts, T., R., G., 2017. Spectral irradiance effects on the outdoor performance of photovoltaic modules. Renewable and Sustainable Energy Reviews 69, 429 – 434. doi:https://doi.org/10.1016/j.rser.2016.10.062.

Figgis, B., Abdallah, A., 2019. Investigation of pv yield differences in a desert climate. Sol. Energy 194, 136–140. https://doi.org/10.1016/j.solener.2019.10.044.

Gilbert, R.O., 1987. Statistical methods for environmental pollution monitoring. John Wiley & Sons.

Goossens, D., Goverde, H., Catthoor, F., 2018. Effect of wind on temperature patterns, electrical characteristics, and performance of building-integrated and building-applied inclined photovoltaic modules. Sol. Energy 170, 64–75. https://doi.org/10.1016/j.solener.2018.05.043.

Green, M.A., 1982. Solar cells: operating principles, technology, and system applications. ph.

Green, M.A., 2003. General temperature dependence of solar cell performance and implications for device modelling. Prog. Photovoltaics Res. Appl. 11, 333–340. https://doi.org/10.1002/pip.496.

Henry, C.H., 1980. Limiting efficiencies of ideal single and multiple energy gap terrestrial solar cells. J. Appl. Phys. 51, 4494–4500. https://doi.org/10.1063/1.328272.

Herteleer, B., Huyck, B., Catthoor, F., Driesen, J., Cappelle, J., 2017. Normalised efficiency of photovoltaic systems: Going beyond the performance ratio. Sol. Energy 157, 408–418. https://doi.org/10.1016/j.solener.2017.08.037.

Hussain, M., Mahmud, I., 2019. pymannkendall: a python package for non parametric mann kendall family of trend tests. Journal of Open Source Software 4, 1556. https://doi.org/10.21105/joss.01556. URL: 10.21105/joss.01556.

IEC, 2009. Iec 60891: Procedures for temperature and irradiance corrections to measured IV characteristics of crystalline silicon photovoltaic devices. 2.

IEC, 2017. Iec 61724: Photovoltaic system performance.

IEC, 2019. International electrotechnical commission 60904–7: Computation of Spectral Mismatch Error Introduced in the Testing of a Photovoltaic Device.

IEC, 2020. Iec 60904–9.

Imenes, A.G., Sclj, J., 2017. Irradiance and temperature distributions at high latitudes: Design implications for photovoltaic systems. In: 2017 IEEE 44th Photovoltaic Specialist Conference (PVSC), pp. 619–625. https://doi.org/10.1109/PVSC.2017.8366376.

Imenes, A.G., Yordanov, G.H., Midtgård, O.M., Saetre, T.O., 2011. Development of a test station for accurate in situ i–v curve measurements of photovoltaic modules in southern norway. In: 2011 37th IEEE Photovoltaic Specialists Conference, pp. 003153–003158.

Ishii, T., Otani, K., Takashima, T., 2011. Effects of solar spectrum and module temperature on outdoor performance of photovoltaic modules in round-robin measurements in Japan. Prog. Photovoltaics Res. Appl. 19, 141–148. https://doi.org/10.1002/pip.995.

Jordan, D.C., Kurtz, S.R., 2014. The dark horse of evaluating long-term field performance—data filtering. IEEE Journal of Photovoltaics 4, 317–323.

Kendall, M., 1975. Rank correlation methods, (4th edn.). charles griffin, San Francisco. CA 8.

King, D., Kratochvil, J., Boyson, W., 1997. Temperature coefficients for PV modules and arrays: measurement methods, difficulties, and results, in: Conference Record of the Twenty Sixth IEEE Photovoltaic Specialists Conference - 1997, IEEE. pp. 1183–1186. doi:10.1109/PVSC.1997.654300.

Kontges, M., Kurtz, S., Packard, C., Jahn, U., Berger, K., Kato, K., Friesen, T., Liu, H., Isehegam, M., 2014. Review of failures of Photovoltaic modules. Technical Report. International Energy Agency, PVPS-Task 13.

Landis, G.A., 1994. Review of solar cell temperature coefficients for space, in: XIII Space Photovoltaic Research and Technology Conference (SPRAT XIII), p. 385.

Louwen, A., de Waal, A.C., Schropp, R.E.I., Faaij, A.P.C., van Sark, W., 2017. Comprehensive characterisation and analysis of PV module performance under real operating conditions. Prog. Photovoltaics Res. Appl. 25, 218–232. https://doi.org/10.1002/pip.2848.

Louwen, A., Waal, A.C.d., van Sark, W., 2016. Evaluation of different indicators for representing solar spectral variation. In: 2016 IEEE 43rd Photovoltaic Specialists Conference (PVSC), pp. 133–137. https://doi.org/10.1109/PVSC.2016.7749563.

Luque, A., Hegedus, S., 2011. Handbook of photovoltaic science and engineering. John Wiley & Sons.

Magare, D., Sastry, O., Gupta, R., Betts, T.R., Gottschalg, R., Kumar, A., Bora, B., Singh, Y., 2016. Effect of seasonal spectral variations on performance of three different photovoltaic technologies in india. International Journal of Energy and Environmental Engineering 7, 93–103.

Mahmood, F., Majeed, H., Agha, H., Ali, S., Tatapudi, S., Curtis, T., TamizhMani, G., 2017. Temperature coefficient of power (Pmax) of field aged PV modules: impact on performance ratio and degradation rate determinations. In: Dhere, N.G., Sakurai, K., Kempe, M.D. (Eds.), Reliability of Photovoltaic Cells, Modules, Components, and Systems X. International Society for Optics and Photonics. SPIE, pp. 52–58. https://doi.org/10.1117/12.2281840.

Malvoni, M., Kumar, N.M., Chopra, S.S., Hatziargyriou, N., 2020. Performance and degradation assessment of large-scale grid-connected solar photovoltaic power plant in tropical semi-arid environment of india. Sol. Energy 203, 101–113. https://doi.org/10.1016/j.solener.2020.04.011.

Mann, H.B., 1945. Nonparametric tests against trend. Econometrica: Journal of the econometric society 245–259.

Mihaylov, B., Bowers, J., Betts, T., Gottschalg, R., Krametz, T., Leidl, R., Berger, K., Zamini, S., Dekker, N., Graditi, G., et al., 2014. Results of the sophia module intercomparison part-1: stc, low irradiance conditions and temperature coefficients measurements of c-si technologies.

Minemoto, T., Nagae, S., Takakura, H., 2007. Impact of spectral irradiance distribution and temperature on the outdoor performance of amorphous si photovoltaic modules. Sol. Energy Mater. Sol. Cells 91, 919–923. https://doi.org/10.1016/j.solmat.2007.02.012.

Mitterhofer, S., Glažar, B., Jankovec, M., Topic, M., 2019. The development of thermal coefficients of photovoltaic devices. Journal of Microelectronics, Electronic Components and Materials 49, 219–227. https://doi.org/10.33180/InfMIDEM2019.404.

Müllejans, H., Wagner, T., Merli, F., Jäger-Waldau, A., Dunlop, E., 2004. Changes in spectral response with temperature and irradiance intensity. Thin Solid Films 451–452, 145–151. https://doi.org/10.1016/j.tsf.2003.11.006.

Osterwald, C.R., Campanelli, M., Kelly, G.J., Williams, R., 2015. On the reliability of photovoltaic short-circuit current temperature coefficient measurements. In: 2015 IEEE 42nd Photovoltaic Specialist Conference (PVSC), pp. 1–6.

Paudyal, B.R., Imenes, A.G., 2019. Performance assessment of field deployed multi-crystalline pv modules in nordic conditions. In: 2019 IEEE 46th Photovoltaic Specialists Conference (PVSC), pp. 1377–1383.

Paudyal, B.R., Imenes, A.G., Saetre, T.O., 2018. Review of guidelines for pv systems performance and degradations monitoring. In: Proceedings of the 35th European

Photovoltaic Solar Energy Conference, pp. 2037–2050. https://doi.org/10.4229/35thEUPVSEC20182018-6DV.1.32.

Pern, F.J., Czanderna, A.W., Emery, K.A., Dhere, R.G., 1991. Weathering degradation of eva encapsulant and the effect of its yellowing on solar cell efficiency, in: The Conference Record of the Twenty-Second IEEE Photovoltaic Specialists Conference - 1991, pp. 557–561 vol 1.

Peters, I.M., Buonassisi, T., 2021. How changes in worldwide operating conditions affect solar cell performance. Sol. Energy 220, 671–679. https://doi.org/10.1016/j.solener.2021.01.017.

Riesen, Y., Stuckelberger, M., Haug, F.J., Ballif, C., Wyrsch, N., 2016. Temperature dependence of hydrogenated amorphous silicon solar cell performances. J. Appl. Phys. 119, 044505. https://doi.org/10.1063/1.4940392.

Rodrigo, P.M., Fernández, E.F., Almonacid, F.M., Pérez-Higueras, P.J., 2017. Quantification of the spectral coupling of atmosphere and photovoltaic system performance: Indexes, methods and impact on energy harvesting. Sol. Energy Mater. Sol. Cells 163, 73–90. https://doi.org/10.1016/j.solmat.2017.01.018.

Sen, P.K., 1968. Estimates of the regression coefficient based on kendall's tau. Journal of the American statistical association 63, 1379–1389.

Senturk, A., 2020. Investigation of datasheet provided temperature coefficients of photovoltaic modules under various sky profiles at the field by applying a new validation procedure. Renewable Energy 152, 644–652. https://doi.org/10.1016/j.renene.2020.01.069.

Sharma, M., Das, N., Helwig, A., Ahfock, T., 2017. Impact of incident light angle on the conversion efficiency of nano-structured gaas solar cells. In: 2017 Australasian Universities Power Engineering Conference (AUPEC), pp. 1–4. https://doi.org/10.1109/AUPEC.2017.8282411.

Shockley, W., Queisser, H.J., 1961. Detailed balance limit of efficiency of p-n junction solar cells. J. Appl. Phys. 32, 510–519. https://doi.org/10.1063/1.1736034.

Siddique, H.A.B., Xu, P., De Doncker, R.W., 2013. Parameter extraction algorithm for one-diode model of pv panels based on datasheet values. In: 2013 International Conference on Clean Electrical Power (ICCEP), pp. 7–13. https://doi.org/10.1109/ICCEP.2013.6586957.

Silverman, T., Friesen, G., Pravettoni, M., Apolloni, M., Louwen, A., Van Sark, W., Schweiger, M., Belluardo, G., Wagner, J., Tetzlaff, A., Ingenhoven, P., Moser, D., Jahn, U., 2014. Characterisation of Performance of Thin-film Photovoltaic Technologies. Technical Report. International Energy Agency, PVPS-Task 13.

Simioni, T., Schaeffer, R., 2019. Georeferenced operating-efficiency solar potential maps with local weather conditions – an application to brazil. Sol. Energy 184, 345–355. https://doi.org/10.1016/j.solener.2019.04.006.

Tayyib, M., Ove, J., Oskar, T., 2014. Irradiance dependent temperature coefficients for MC solar cells from Elkem solar grade silicon in comparison with reference polysilicon. Energy Procedia 55, 602–607. https://doi.org/10.1016/j.egypro.2014.08.032.

Theristis, M., Venizelou, V., Makrides, G., Georghiou, G.E., 2018. Energy yield in photovoltaic systems. In: Kalogirou, S.A. (Ed.), McEvoy's Handbook of Photovoltaics (Third Edition), third edition ed. Academic Press, pp. 671–713. https://doi.org/10.1016/B978-0-12-809921-6.00017-3.

Wang, F., Shao, W., Yu, H., Kan, G., He, X., Zhang, D., Ren, M., Wang, G., 2020. Re-evaluation of the power of the mann-kendall test for detecting monotonic trends in hydrometeorological time series. Frontiers in Earth Science 8, 14. https://doi.org/10.3389/feart.2020.00014.

Ziane, A., Necaibia, A., Sahouane, N., Dabou, R., Mostefaoui, M., Bouraiou, A., Khelifi, S., Rouabhia, A., Blal, M., 2021. Photovoltaic output power performance assessment and forecasting: Impact of meteorological variables. Sol. Energy 220, 745–757. https://doi.org/10.1016/j.solener.2021.04.004.